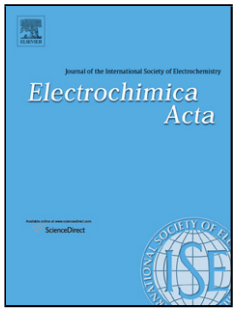

Title: Hierarchical (Ni,Co)Se_2/Carbon Hollow Rhombic Dodecahedra Derived from Metal-Organic Frameworks for Efficient Water-Splitting Electrocatalysis

Authors: Fangwang Ming, Hanfeng Liang, Huanhuan Shi, Gui Mei, Xun Xu, Zhoucheng Wang

PII: S0013-4686(17)31686-9
DOI: http://dx.doi.org/doi:10.1016/j.electacta.2017.08.047
Reference: EA 30051

To appear in: *Electrochimica Acta*

Received date: 22-5-2017
Revised date: 3-8-2017
Accepted date: 8-8-2017

Please cite this article as: Fangwang Ming, Hanfeng Liang, Huanhuan Shi, Gui Mei, Xun Xu, Zhoucheng Wang, Hierarchical (Ni,Co)Se2/Carbon Hollow Rhombic Dodecahedra Derived from Metal-Organic Frameworks for Efficient Water-Splitting Electrocatalysis, Electrochimica Actahttp://dx.doi.org/10.1016/j.electacta.2017.08.047

Hierarchical (Ni,Co)Se_2/Carbon Hollow Rhombic Dodecahedra Derived from Metal-Organic Frameworks for Efficient Water-Splitting Electrocatalysis

Fangwang Ming[†], *Hanfeng Liang,**[,‡] *Huanhuan Shi*[†], *Gui Mei*[†], *XunXu*[†], *Zhoucheng Wang**[,†]

[†]College of Chemistry and Chemical Engineering, Xiamen University, Xiamen 361005, China

[‡]Materials Science and Engineering, King Abdullah University of Science and Technology (KAUST), Thuwal 23955-6900, Saudi Arabia

E-mail: zcwang@xmu.edu.cn (Z. Wang); hanfeng.liang@kaust.edu.sa (H. Liang)

Abstract: In this work, we demonstrate that the electrocatalytic activity of transition metal chalcogenides can be greatly enhanced by simultaneously engineering the active sites, surface area, and conductivity. Using metal-organic frameworks-derived (Ni,Co)Se_2/C hollow rhombic dodecahedra (HRD) as a demonstration, we show that the incorporation of Ni into $CoSe_2$ could generates additional active sites, the hierarchical hollow structure promotes the electrolyte diffusion, the *in-situ* hybridization with C improves the conductivity. As a result, the (Ni,Co)Se_2/C HRD exhibit superior performance toward the overall water-splitting electrocatalysis in 1 M KOH with a cell voltage as low as 1.58 V at the current density of 10 mA cm^{-2}, making the (Ni,Co)Se_2/C HRD as a promising alternative to noble metal catalysts for water splitting.

Keywords: metal-organic frameworks, $Ni_{0.67}Co_{0.33}Se_2$/C, hydrogen evolution reaction (HER), oxygen evolution reaction (OER), water-splitting electrocatalysis

1. Introduction

Facing the increasingly serious environmental problems and energy crisis, developing clean and sustainable alternatives to fossil fuels is a matter of utmost urgency. Hydrogen, which is regarded as a clean energy carrier, has the potential to take place of the rapidly dwindling fossil fuels. Water splitting provides one of the most promising pathways for high-purity hydrogen generation. However, it is an uphill process and thus requires external energies (237 kJ mol^{-1}) to initiate the reaction [1, 2]. In an electrochemical water splitting system, the reaction rate can be accelerated by efficient electrocatalysts that can expedite the sluggish kinetics of the two half reactions, namely the cathodic hydrogen evolution reaction (HER) and the anodic oxygen evolution reaction (OER) [3-5]. The state-of-the-art Pt-based HER catalysts and Ru- or Ir-based OER catalysts suffer from scarcity and high cost, which seriously limit their widespread adoption. Motivated by this challenge, the development of robust and cost-efficient catalysts with high activity is crucial for the hydrogen economy and has achieved remarkable progress [6-12].

Transition metal chalcogenides (TMCs) have recently attracted extensive research interest owing to their high activity toward both the HER and OER [4, 13-18]. Among them, Co- or Ni-based selenides with high catalytic activity, small Tafel slope and long-term stability have been identified as promising low cost electrocatalysts for water splitting. Previous studies demonstrated that the chalcogenide atoms at the edges of $CoSe_2$ and $NiSe_2$ are electrochemical active sites, similar to the case of MoS_2 [19, 20]. From this perspective, the key point for optimizing the catalytic performance of TMCs is to maximize the exposed edge sites. A series of techniques have been proposed to boost the catalytic activity by manipulating the exposed active sites on nanoscale and atomic scale, which includes: I) Nanostructuring. Nanowires, ultrathin

nanosheets, porous/hollow structures, and hierarchical architectures with large surface area generally have more exposed active edge sites [6-13]. In particular, hollow structures have attracted much attention in catalysis because of their interesting features such as large surface area, low density, kinetically favorable open structure, and surface permeability [21-23]. II) Elemental doping. Generally elemental doping could tune the electronic structure and thus the chemical and physical properties, resulting in enhanced activity and stability, and sometimes also exposure of more active sites. For instance, Xie et al. demonstrated that Mn doping into $CoSe_2$ distorts the atomic arrangement and thus generates additional edge active sites [20]. III) Besides active sites engineering, hybridizing TMCs with conductive carbon materials could also improve the catalytic performance [24-26]. These materials not only enhance the electrical conductivity but also prevent the aggregation of the nanoparticles and further alleviate the structural evolution during the electrochemical reactions [27]. Notwithstanding enormous efforts have been made to enhance the catalytic performance of TMCs, their efficiency toward the water splitting still exist a certain disparity with noble metal catalysts.

In this work, we integrate all the three strategies together to enhance the electrocatalytic activity of a metal-organic frameworks (MOFs)-derived (Ni,Co)Se_2/C hollow rhombic dodecahedra (HRD) catalyst. The introduction of Ni into $CoSe_2$ generates a subtle distortion in the lattice because of the mismatch in their Jahn-Teller distortion degrees (i.e., Ni^{2+}, $t_{2g}^6e_g^2$, no Jahn-Teller effect; Co^{2+}, $t_{2g}^6e_g^1$, strong Jahn-Teller effect), and thus creates more active sites [20]. The unique hollow structure with edge-to-face stacking shells allows the close contact with electrolytes and enables large surface area. The C layer improves the conductivity but also serves as a buffer layer to release the strain formed by the structural evolution during the electrocatalysis [7-9, 12]. By simultaneously engineering the active sites, surface area, and

conductivity, the obtained (Ni,Co)Se_2/C HRD show good electrocatalytic activity towards both the HER and OER in alkalinesolution. Moreover, it also achieves stable performance toward the overall water splitting with a cell voltage as low as 1.58 V at the current density of 10 mA cm^{-2}.

2. Experimental Section

2.1. MaterialsPreparation

2.1.1. Synthesis of zeolitic imidazolate framework-67 (ZIF-67): All the chemicals were directly used after purchase without purification. In a typical synthesis, 1 mmol of $Co(NO_3)_2 \cdot 6H_2O$ and 4 mmol of 2-methylimidazole were dissolved in 25 mL of methanol, respectively. Then, solution of 2-methylimidazole was quickly poured into the solution of $Co(NO_3)_2$ under vigorous stirring. The well mixed solution was aged for 24 h at room temperature. Finally, the purplep recipitate of ZIF-67 was washed with ethanol for several times by centrifugation, and then dried at 60 °C for 6 h [28].

2.1.2. Synthesis of NiCo Layered Double Hydroxide (LDH) and CoCo LDH: 40 mg of ZIF-67 was first dispersed in 20 mL of ethanol, and then 5 mL of ethanol solution containing 90 mg of $Ni(NO_3)_2 \cdot 6H_2O$ was quickly poured into the former purple dispersion. Then the mixture was refluxed for 1 h under stirring. After that, the product was washed with ethanol for 3 times by centrifugation and dried at 60 ºC for 6 h. As for CoCo LDH, the $Ni(NO_3)_2$ was replaced by 100 mg $Co(NO_3)_2$ with other conditions unchanged.

2.1.3. Synthesis of $CoSe_2$/NC-SRD (N-doped Carbon-Solid Rhombic Dodecahedra), (Ni,Co)Se_2/C-HRD and $CoSe_2$/C-HRD: The as-synthesized ZIF-67 was converted into $CoSe_2$/NC-SRD using a horizontal quartz tube furnace. 0.1 g of ZIF-67 and 0.5 g of Se powder were placed at the downstream and upstream sides of the tube furnace, respectively. The furnace

was heated to 400 °C for 2 h with a heating ramp of 2 °C min^{-1} in N_2 atmosphere. During the whole process, the flow of N_2 was maintained at a rate of 100 sccm. As for (Ni,Co)Se_2/C-HRD and $CoSe_2$/C-HRD, the ZIF-67 was replaced by 0.1 g of NiCo LDH and CoCo LDH, respectively, with other conditions unchanged. For comparison, the samples prepared at 350 °C and 450 °C for (Ni,Co)Se_2/C-HRD were also produced.

2.1.4. Preparation of $CoSe_2$/NC-SRD, (Ni,Co)Se_2/C-HRD, and $CoSe_2$/C-HRD electrodes: The as-synthesized samples were prepared by ultrasonically mixing 4 mg of the catalyst powder with the mixture of 40 μL 5% Nafion solution, 560 μL ethanol and 400 μL H_2O for 15 min to form homogeneous catalyst ink. Next, a certain volume of the ink was carefully dropped onto the clean Ni foam (NF), leading to a desirable catalyst loading. The catalyst loading was about 1.5 mg cm^{-2}.

2.1.5. Preparation of Pt/C/NF, RuO_2/NFand IrO_2/NF electrodes: The commercial 20 wt.% Pt/C, RuO_2 and IrO_2 samples were prepared by ultrasonically mixing 4 mg of the catalyst powder with the mixture of 40 μL 5% Nafion solution, 560 μL ethanol and 400 μL H_2O for 15 min to form homogeneous catalyst ink. Next, a certain volume of the ink was carefully dropped onto the clean NF, leading to a desirable catalyst loading. The catalyst loading was about 1.5 mg cm^{-2}.

2.2. Characterizations: The characterizations of the catalysts were carried out by X-ray diffraction (XRD, Rigaku) with Cu Kα radiation (λ = 1.54056 Å), filed emission scanning electron microscopy (SEM, ZEISS, SIGMA), transmission electron microscopy, high-resolution transmission electron microscopy (HRTEM, Tecnai-F30) and inductively couple plasma mass spectrometry (ICP-MS) (Thermo Fisher, US). X-ray photoelectron spectroscopy (XPS) measurement was performed on PHI Quantum-2000 XPS (US). Raman spectra were recorded

using a Horiba XploRA Confocal Raman microscope fitted with 532 nm excitation laser. Thermogravimetric analysis (TGA) was performed using a SDT-Q600 Thermogravimetric Analyzer in N_2, over a range from room temperature to 800 °C with a ramping rate of 10 °C min^{-1}.

2.3. Electrochemical measurements: All electrochemical measurements were conducted at room temperature in a typical three-electrode or two-electrode configuration using an electrochemical workstation (CHI 660E, CH Instruments, Inc.). The HER and OER performance was evaluated in 1 M KOH (pH=13.6) solution using the as-fabricated electrode as the working electrode, a platinum plate as the counter electrode, and a saturated calomel electrode (SCE) as the reference electrode, respectively. The overall water splitting performance was evaluated in 1 M KOH and 6 M KOH solutions respectively using the as-fabricated electrode as both the anode and the cathode. All polarization curves are *IR*-corrected according to: $E_{corr} = E_{mea} - IR_s$, where E_{corr} is *IR*-corrected potential, E_{mea} is experimentally measured potential, and R_s is the equivalent series resistance extracted from the electrochemical impedance spectroscopy measurement. Unless otherwise specified, all potentials reported are on the reversible hydrogen electrode (RHE) scale by converting the potentials measured versus SCE according to: $E_{(RHE)} = E_{(SCE)} + 0.241 + 0.059$ pH. It should be noted that all electrochemical data in this paper were collected after at least 50 CV cycles to ensure a stable electrochemical performance.

3. Results and Discussion

3.1. Synthesis and Structure of (Ni,Co)Se_2/C-HRD

The (Ni,Co)Se_2/C-HRD were synthesized by a two-step conversion reaction using ZIF-67 as precursor (Fig. 1). Typically, the ZIF-67 rhombic dodecahedra were first converted into NiCo

LDH [28] followed by a thermal selenization (see Experimental section for details). For comparison, $CoSe_2$/C-HRD and $CoSe_2$/N-doped C solid rhombic dodecahedra ($CoSe_2$/NC-SRD) were also synthesized for comparison. The crystal structure and phase purity of ZIF-67, NiCo LDH, and CoCo LDH were confirmed by powder X-ray diffraction (XRD) (Fig. S1). The morphologies and structures of these precursors were then characterized by scanning electron microscope (SEM) and transmission electron microscope (TEM). As shown in Fig. S2a and d, the ZIF-67 is composed of uniform rhombic dodecahedra with an average size of approximately 600 nm. By contrast, the NiCo LDH (Fig. S2b and e) and CoCo LDH (Fig. S2c and f) present similar morphologies as that of ZIF-67 but with hollow interiors. Interestingly, the shells of NiCo LDH are assembled by many thin nanosheets, leading to a highly hierarchical structure with large surface area. Whereas for CoCo LDH, the size of the surface nanosheets is much larger, probably due to the strong affinity between cobalt nitrate and Co-containing template that promotes the growth [28].

After thermal selenization at 400 °C, the three precursors were converted into corresponding selenides with well-retained morphologies. As shown in Fig. 2a, the diffraction peaks of the product converted from NiCo LDH are assigned to $(Ni,Co)Se_2$ solid solution (JCPDS No. 29-1417). Meanwhile, the ZIF-67 and CoCo LDH were successfully converted into orthorhombic marcasite-type $CoSe_2$ (JCPDS No. 53-0449), and cubic pyrite-type phase $CoSe_2$ (JCPDS No. 65-3327), respectively. Raman spectra were conducted to further corroborate the structures of the as-synthesized products. As shown in Fig. 2b, the distinct peaks at 190 and 194 cm^{-1} correspond to the Se-Se stretching mode of cubic and orthorhombic $CoSe_2$, respectively [29-31], whereas the

peak at around 217 cm^{-1} is associated with A_g modes of $NiSe_2$ [32-34]. The broad peaks at ~1348 and ~1582 cm^{-1} are attributed to the D peak and G peak of the amorphous carbon [35, 36], suggesting the existence of carbon that was derived from the organic ligands in ZIF-67. We further carried out X-ray photoelectron spectroscopy (XPS) measurements to probe the surface composition and the chemical oxidation states of the products. Fig. S3 shows the XPS spectra of $CoSe_2$/NC-SRD. The elements of C, N, Co and Se can be detected, where C and N are originated from 2-methylimidazole. The high resolution spectrum of N 1s (Fig. S3b) can be well-fitted into four peaks at 398.2, 399.0, 400.5 and 401.6 eV, corresponding to pyridinic-N, Co-N, pyrrolic-N and graphitic-N, respectively [37, 38]. The Co $2p_{3/2}$ and $2p_{1/2}$ correspond to Co^{2+} species in $CoSe_2$ [39], while the Se 3d peak at 54 and 58 eV can be assigned to the metal-selenium bond and the SeO_x peak caused by the surface oxidation when exposed to air, respectively [30, 39]. The XPS spectra of (Ni,Co)Se_2/C-HRD and $CoSe_2$/C-HRD are displayed in Fig. S4 and S5. There is no detected signal of N, which may be due to the 2-methylimidazole was consumed during the formation of LDHs. The binding energies observed for Co $2p_{3/2}$, Co $2p_{1/2}$, Ni $2p_{3/2}$, and Ni $2p_{1/2}$ peaks are in agreement with those reported for (Ni,Co)Se_2 and $CoSe_2$ [7, 40].

The morphology and structure of the samples were further revealed by SEM and TEM (Fig. 2). It can be observed that all three samples inherit the morphology of their corresponding precursors. Specially, the (Ni,Co)Se_2/C-HRD and $CoSe_2$/C-HRD are composed of nanosheets assembled hollow rhombic dodecahedra (Fig. 2g, h and k, l), whereas the $CoSe_2$/NC-SRD (Fig. 2c, d) has a solid interior. Furthermore, the lattice spacings measured from high resolution TEM (HRTEM) images match the $d_{(200)}$, $d_{(211)}$ and $d_{(220)}$ spacings of orthorhombic $CoSe_2$, (Ni,Co)Se_2 solid solution, and cubic $CoSe_2$, respectively (Fig. 2e, i, and m), in agreement with the XRD results. The high-angle annular dark field (HAADF) images and the associated scanning TEM-

energy dispersive spectroscopy (STEM-EDS) elemental maps (Fig. 2f, j, and n) confirm the uniform distribution of C, N, Co, Ni, and Se of the samples. Inductively coupled plasma mass spectrometry (ICP-MS) analysis revealed that the molar ratio of Ni/Co/Se in (Ni,Co)Se_2/C-HRD is close to 0.67:0.33:2, giving a stoichiometric formula of $Ni_{0.67}Co_{0.33}Se_2$. We further carried out the energy dispersive X-ray (EDX) analysis and the result shows the molar ratio of Co/Se is nearly 1:2 for $CoSe_2$/NC-SRD and $CoSe_2$/C-HRD, consistent with the stoichiometry of the chemical formula (Fig. S6). Combined with the XRD, Raman, XPS, and EDX, it is clear that the (Ni,Co)Se_2/C-HRD as well as the other two $CoSe_2$ nanostructures were formed successfully.

3.2. HER Electrocatalysis

The electrocatalytic activities of the three products for HER were evaluated using a standard three-electrode electrochemical cell in 1 M KOH solution (see Experimental section for details). Polarization curves with *IR*-correction were recorded at 3 mV s^{-1}. As shown in Fig. 3a, high catalytic activities were observed for these selenides. Specifically, the overpotentials required to achieve the current density of 10 mA cm^{-2} are 87, 157, and 189 mV for (Ni,Co)Se_2/C-HRD, $CoSe_2$/C-HRD, and $CoSe_2$/NC-SRD, respectively, while 270 mV for NF. (Ni,Co)Se_2/C-HRD possesses the lowest overpotential that is comparable to commercial Pt/C. In addition, this value compares favorably to NiCo LDH, CoCo LDH (Fig. S7) and most of recent reported earth-abundant HER electrocatalysts under alkaline conditions (see comparisons in Table S1). Their Tafel slopes are determined to be 65, 100, and 115 mV dec^{-1} for (Ni,Co)Se_2/C-HRD, $CoSe_2$/C-HRD and $CoSe_2$/NC-SRD, respectively (Fig. 3b), indicating the HER over the catalysts proceeded by a Volmer-Heyrovsky Mechanism [41, 42]. We also estimated the electrochemically active surface area (ECSA) by using a simple cyclic voltammetry (CV) method (Fig. S8). The extracted double-layer capacitance (C_{dl}) is supposed to be linearly

proportional to the actual effective active surface area in the catalyst materials [9, 43]. As shown in Fig. 3c, (Ni,Co)Se_2/C-HRD possesses the highest C_{dl} of 40.9 mF cm^{-2}, followed by $CoSe_2$/C-HRD and $CoSe_2$/NC-SRD (7.4 and 5.4 mF cm^{-2}, respectively). This trend is in accordance with the catalytic performance towards the HER. Note that the ECSA of (Ni,Co)Se_2/C-HRD is much larger than that of $CoSe_2$/C-HRD despites their quite similar morphology, suggesting that the introduction of heterogeneous spin states, namely Ni, into $CoSe_2$ can greatly increase the surface active sites and thus boost the activity. In an attempt to understand the performance difference of the three materials, we normalized the polarization curves to the ECSA. As shown in Fig. 3d, there is only slight difference between $CoSe_2$/NC-SRD and $CoSe_2$/C-HRD, indicating the same intrinsic activity of these two materials. Therefore, the performance disparity between the two different $CoSe_2$ phasesis attributed to their different surface area because of the different hollowness. Further, the ternary (Ni,Co)Se_2/C-HRD possesses a higher catalytic activity than $CoSe_2$/C-HRD even though they have similar hollow structures. This clearly indicates that the enhancement of the catalytic activity mainly comes from the synergistic effect of Ni and Co. The (Ni,Co)Se_2/C-HRD also exhibits good durability as confirmed by the chronopotentiometric measurement (Fig. S9) and polarization curves which after 2000 CV cycles (Fig. S10). The overpotential required to deliver 20 mA cm^{-2} shows negligible changes upon 36 h operation. The stability was further supported by the SEM and HRTEM images (Fig. S11), which reveal that the morphology and the phase of (Ni,Co)Se_2/C-HRD remain unchanged after the HER.

3.3. OER Electrocatalysis

We next assessed the OER performance of three as-obtained products in the same electrolyte (1 M KOH). As shown in Fig. 4a, similarly, the (Ni,Co)Se_2/C-HRD demonstrate a much smaller

overpotential of 245 mV to deliver a current density of 10 mA cm^{-2} than that of $CoSe_2$/C-HRD (295 mV) and $CoSe_2$/NC-SRD (300 mV). This low overpotential compares favorably to NiCo LDH, CoCo LDH (Fig. S12) and those recently reported high-performance non-noble metal OER catalysts (see comparison in Table S2), and even exceeds the commercial RuO_2 or IrO_2 catalyst, making it a promising alternative for OER. The (Ni,Co)Se_2/C-HRD also possesses the smallest Tafel slope (70 mV dec^{-1}), followed by $CoSe_2$/C-HRD (72 mV dec^{-1}) and $CoSe_2$/NC-SRD (98 mV dec^{-1}) (Fig. 4b), manifesting a more favorable OER kinetics. Furthermore, the polarization curves (Fig. S13) for the (Ni,Co)Se_2/C-HRD show the catalytic OER currents barely change with scan rates increase from 0.5 to 5 mV s^{-1}, implying the efficient charge and mass transport during the catalytic process [44]. We also measured the C_{dl} (Fig. 4c and S14) and the result shows that the (Ni,Co)Se_2/C-HRD possess the highest C_{dl} of 54.4 mF cm^{-2}, which means more active sites are exposed. We further normalized the current density to ECSA (Fig. 4d), similar as we observed during HER measurements, the result again confirms that the hollow structure and the synergy effect have positive impacts on the electrocatalytic performance. Besides the high activity, the (Ni,Co)Se_2/C-HRD also show good stability upon long-term OER test. The potential at 20 mA cm^{-2} only slightly increases from 270 to 273 mV after 36 h (Fig. S9). The SEM and TEM measurements (Fig. S15) further reveal that the structure is well retained. We noted that recent reports have suggested an oxidation occurs on the surface of selenide-based catalysts during the OER [7, 45, 46]. We therefore performed XPS to confirm the chemical state of the catalyst after OER (Fig. S16). Comparing with the original material (Fig. S4), it is obviously that there are some peaks emerged, which are responsible for Co-O and Ni-O bonding, indicating the formation of oxyhydroxide [7, 46, 47]. The increase of SeO_x peak intensity and the decrease of the Se 3d peak (Fig. S16d) indicate that the Se species at the surface of (Ni,Co)Se_2

solid solution are oxidized, which are accordance with the previous reports [46, 48]. These results suggest that the real active sites for OER are the surface *in situ* generated NiCo oxyhydroxides. We also investigated the effect of thermal selenization temperature (350, 400, and 450 °C) on the electrocatalytic activity of (Ni,Co)Se_2/C-HRD. The XRD analysis confirms that the three samples obtained at different temperatures are phase pure (Ni,Co)Se_2 solid solution (Fig. S17). The electrochemical measurement result shows that the (Ni,Co)Se_2/C-HRD-400 °C exhibits the lowest overpotentials and the smallest Tafel slopes for both the HER and OER (Fig. S18). The superior performance can be attributed to the different ECSA (Fig. S18c, f).

3.4. Overall Water-Splitting Performance

Encouraged by the good HER and OER electrocatalytic activity achieved on (Ni,Co)Se_2/C-HRD, we then assembled a two-electrode configuration using (Ni,Co)Se_2/C-HRD as both anode and cathode for overall water splitting in 1 M KOH. The NF, $CoSe_2$/NC-SRD, $CoSe_2$/C-HRD as well as Pt/C||RuO_2 were also examined for comparison. Fig. 5a shows the *IR*-corrected polarization curves. The (Ni,Co)Se_2/C-HRD electrode shows excellent activity with 10 mA cm^{-2} water-splitting current density reached at a cell voltage as low as 1.58 V. This value is close to that of noble metal catalysts Pt/C||RuO_2 (1.55 V) and Pt/C||IrO_2 (1.575 V), and compares favorably to $CoSe_2$/C-HRD (1.63 V), $CoSe_2$/NC-SRD (1.68 V), and previously reported catalysts under similar conditions (see Table S3). Furthermore, the (Ni,Co)Se_2/C-HRD is very stable for at least 48 h (Fig. 5b). The superior catalytic performance of (Ni,Co)Se_2/C-HRD in overall water-splitting are ascribed to the synergistic effect of Co and Ni as well as the unique hollow structure with edge-to-face stacking nanosheets-assembled shell. The incorporation of Ni into $CoSe_2$ exposes additional active sites. The unique hierarchical hollow structure provides a large active surface area, which not only promotes the diffusion and penetration of electrolyte but also

facilitates gas bubble release and surface electrochemical reactions. In addition, the *in-situ* hybridized carbon also improves the conductivity and buffers the structure evolution during the electrocatalysis, leading to a high activity and stability. We further assessed the catalytic performance and durability of (Ni,Co)Se_2/C-HRD in concentrated alkaline (6 M KOH) solution to meet the requirement of industrial production. As shown in Fig. S19, the (Ni,Co)Se_2/C-HRD exhibits excellent activities for HER (only needs -41 mV to deliver 10 mA cm^{-2} and -109 mV to achieve 100 mA cm^{-2}, Fig. S19a), OER (260 mV for 100 mA cm^{-2}, Fig. S19b) and overall water-splitting (1.66 and 1.71 V for 50 and 100 mA cm^{-2}, respectively, Fig. S19c). Besides, the as-obtained (Ni,Co)Se_2/C-HRD also shows good durability in 6 M KOH, as only deduced 4.22 % (from 49.7 to 47.6 mA cm^{-2}) under a static potential of 1.66 V vs. RHE for 20 h.

4. Conclusions

In summary, we report a general strategy of greatly enhancing the electrocatalytic activity of selenides by simultaneously engineering the active sites, surface area, and conductivity. Using (Ni,Co)Se_2 as a demonstration, we show that the introduction of heterogeneous Ni spin states, construction of hierarchical hollow structure, and *in situ* hybridization with carbon could largely boost the electrocatalytic activity toward both the HER and OER. As a result, the (Ni,Co)Se_2/C hollow rhombic dodecahedra (HRD) derived from metal-organic frameworks precursor show superior performance toward the overall water-splitting that only requires a cell voltage as low as 1.58 V to deliver the current density of 10 mA cm^{-2} along with outstanding stability. Our work not only establishes (Ni,Co)Se_2/C HRD as a promising electrocatalyst for water splitting but may also open up a new route to the rational design of transition metal selenides and further to enhance their performance in electrocatalysis and many other applications.

Acknowledgements

The authors thank the National Natural Science Foundation of China (No. 51372212) for financial support.

Appendix A. Supplementary data

Supplementary data associated with this article can be found, in the online version, at http://

References

[1] F. Wang, T.A. Shifa, X. Zhan, Y. Huang, K. Liu, Z. Cheng, C. Jiang, J. He, Nanoscale, 7 (2015) 19764-19788.

[2] X. Zou, Y. Zhang, Chem. Soc. Rev. 44 (2015) 5148-5180.

[3] Y. Jiao, Y. Zheng, M. Jaroniec, S.Z. Qiao, Chem. Soc. Rev. 44 (2015) 2060-2086.

[4] M.S. Faber, S. Jin, Energy Environ. Sci. 7 (2014) 3519-3542.

[5] W.T. Hong, M. Risch, K.A. Stoerzinger, A. Grimaud, S. Jin, S.H. Yang, Energy Environ. Sci. 8 (2015) 1404-1427.

[6] H. Shi, H. Liang, F. Ming, Z. Wang, Angew. Chem. Int. Ed. 56 (2017) 573-577.

[7] F. Ming, H. Liang, H. Shi, X. Xu, G. Mei, Z. Wang, J. Mater. Chem. A 4 (2016) 15148-15155.

[8] H. Liang, A.N. Gandi, D.H. Anjum, X. Wang, U. Schwingenschlögl, H.N. Alshareef, Nano Lett. 16 (2016) 7718-7725.

[9] H. Liang, H. Shi, D. Zhang, F. Ming, R. Wang, J. Zhuo, Z. Wang, Chem. Mater. 28 (2016) 5587-5591.

[10] H. Liang, L. Li, F. Meng, L. Dang, J. Zhuo, A. Forticaux, Z. Wang, S. Jin, Chem. Mater. 27 (2015) 5702-5711.

[11] H. Liang, F. Meng, M. Cabán-Acevedo, L. Li, A. Forticaux, L. Xiu, Z. Wang, S. Jin, Nano let. 15 (2015) 1421-1427.

[12] H. Liang, A.N. Gandi, C. Xia, M.N. Hedhili, D.H. Anjum, U. Schwingenschlög, H.N. Alshareef, ACS Energy Lett. 2 (2017) 1035-1042.

[13] S. Anantharaj, J. Kennedy, S. Kundu, ACS Appl. Mater. Interfaces 9 (2017) 8714-8728.

[14] L. Yang, H. Hong, Q. Fu, Y. Huang, J. Zhang, X. Cui, Z. Fan, K. Liu, B. Xiang, ACS Nano 9 (2015) 6478.

[15] Y. Guo, J. Tang, H. Qian, Z. Wang, Y. Yamauchi, Chem. Mater. 29 (2017) 5566–5573.

[16] X. Huang, Chem. Soc. Rev. 42 (2013) 1934-1946.

[17] M.R. Gao, M.K. Chan, Y. Sun, Nature Commun. 6 (2015) 7493.

[18] M. Zeng, Y. Li, J. Mater. Chem. A 3 (2015) 14942-14962.

[19] F. Wang, Y. Li, T.A. Shifa, K. Liu, F. Wang, Z. Wang, P. Xu, Q. Wang, J. He, Angew. Chem. Int. Ed. 55 (2016) 6919-6924.

[20] Y. Liu, X. Hua, C. Xiao, T. Zhou, P. Huang, Z. Guo, B. Pan, Y. Xie, J. Am. Chem. Soc. 138 (2016) 5087-5092.

[21] K. An, S.G. Kwon, M. Park, H.B. Na, S.I. Baik, J.H. Yu, D. Kim, J.S. Son, Y.W. Kim, I.C. Song, Nano Lett. 8 (2008) 4252-4258.

[22] D.J. Martin, K. Qiu, S.A. Shevlin, A.D. Handoko, X. Chen, Z. Guo, J. Tang, Angew. Chem. Int. Ed. 53 (2014) 9240-9245.

[23] H. Liang, W. Chen, X. Jiang, X. Xu, B.Xu, Z. Wang, J. Mater. Chem. A 2 (2014) 4340-4346.

[24] T. Meng, J. Qin, S. Wang, D. Zhao, B. Mao M. Cao, J. Mater. Chem. A 5 (2017) 7001-7014.

[25] S. Li, S.Peng, L. Huang, X. Cui, A.M. Al-Enizi, G. Zheng, ACS Appl. Mater. Interfaces 8 (2016) 20534-20539.

[26] Z. Tao, T. Wang, X. Wang, J. Zheng, X. Li, ACS Appl. Mater. Interfaces 8 (2016) 35390-35397.

[27] Y. Li, H. Wang, L. Xie, Y. Liang, G. Hong, H. Dai, J. Am. Chem. Soc. 133 (2011) 7296-7299.

[28] Z. Jiang, Z. Li, Z. Qin, H. Sun, X. Jiao, D. Chen, Nanoscale 5 (2013) 11770-11775.

[29] L. Zhu, M. Teo, P.C. Wong, K.C. Wong, I. Narita, F. Ernst, K.A.R. Mitchell, S.A. Campbell, Appl. Catal. A 386 (2010) 157-165.

[30] D. Kong, H. Wang, Z. Lu, Y. Cui, J. Am. Chem. Soc. 136 (2014) 4897-4900.

[31] K. Zhang, M. Park, L. Zhou, G.H. Lee, W. Li, Y.M. Kang, J. Chen, Adv. Funct. Mater. 36 (2016) 6728-6735.

[32] H. Zhou, Y. Wang, R. He, F. Yu, J. Sun, F. Wang, Y. Lan, Z. Ren, S. Chen, Nano Energy 20 (2016) 29-36.

[33] D. Kong, J.J. Cha, H. Wang, H.R. Lee, Y. Cui, Energy Environ. Sci. 6 (2013) 3553-3558.

[34] C.D.L. Heras, F. Agull-Rueda, J. Phys. Condens. Matter 12 (2000) 5317-5324.

[35] A.C. Ferrari, J. Robertson, Phys. Rev. B: Condens. Matter 61 (2000) 14095-14107.

[36] X.F. Luo, C.H. Yang, Y.Y. Peng, N.W. Pu, M.D. Ger, C.T. Hsieh, J.K. Chang, J. Mater. Chem. A 3 (2015) 10320-10326.

[37] Z. Zhang, J. Hao, W. Yang, J. Tang, ChemCatChem 7 (2015) 1920-1925.

[38] X. Li, Z. Niu, J. Jiang, L. Ai, J. Mater. Chem. A 4 (2016) 3204-3209.

[39] I.H. Kwak, H.S. Im, D.M. Jang, Y.W. Kim, K. Park, Y.R. Lim, E.H. Cha, J. Park, ACS Appl. Mater. Interfaces 8 (2016) 5327-5334.

[40] T. Liu, A.M. Asiri, X. Sun, Nanoscale 8 (2016) 3911-3915.

[41] X. Gao, H. Zhang, Q. Li, X. Yu, Z. Hong, X. Zhang, C. Liang, Z. Lin, Angew. Chem. Int. Ed. 55 (2016) 6290-6294.

[42] E. Skúlason, V. Tripkovic, M.E. Björketun, S. Gudmundsdóttir, G. Karlberg, J. Rossmeisl, T. Bligaard, H. Jónsson, J.K. Nørskov, J. Phys. Chem. C 114 (2010) 18182-18197.

[43] M. Cabán-Acevedo, M.L. Stone, J.R. Schmidt, J.G. Thomas, Q. Ding, H.C. Chang, M.L. Tsai, J.H. He, S. Jin, Nature Mater.14 (2015) 1245.

[44] S. Chen, J. Duan, J. Ran, M. Jaroniec, S.Z. Qiao, Energy Environ. Sci. 6 (2013) 3693-3699.

[45] R. Xu, R. Wu, Y. Shi, J. Zhang, B. Zhang, Nano Energy, 24 (2016) 103-110.

[46] C. Tang, N. Cheng, Z. Pu, W. Xing, X. Sun, Angew. Chem. Int. Ed. 54 (2015) 9351-9355.

[47] J. Yang, H. Liu, W.N. Martens, R.L. Frost, J. Phys. Chem. C, 114 (2010) 923–937.

[48] C. Xia, Q. Jiang, C. Zhao, M.N. Hedhili, H.N. Alshareef, Adv. Mater. 28 (2015) 77-85.

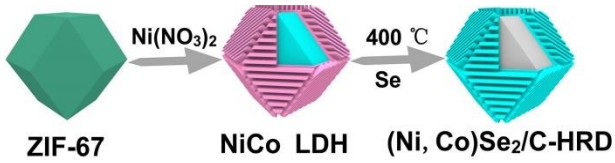

Fig. 1. Schematic illustration of the synthesis of (Ni, Co)Se_2/C-HRD.

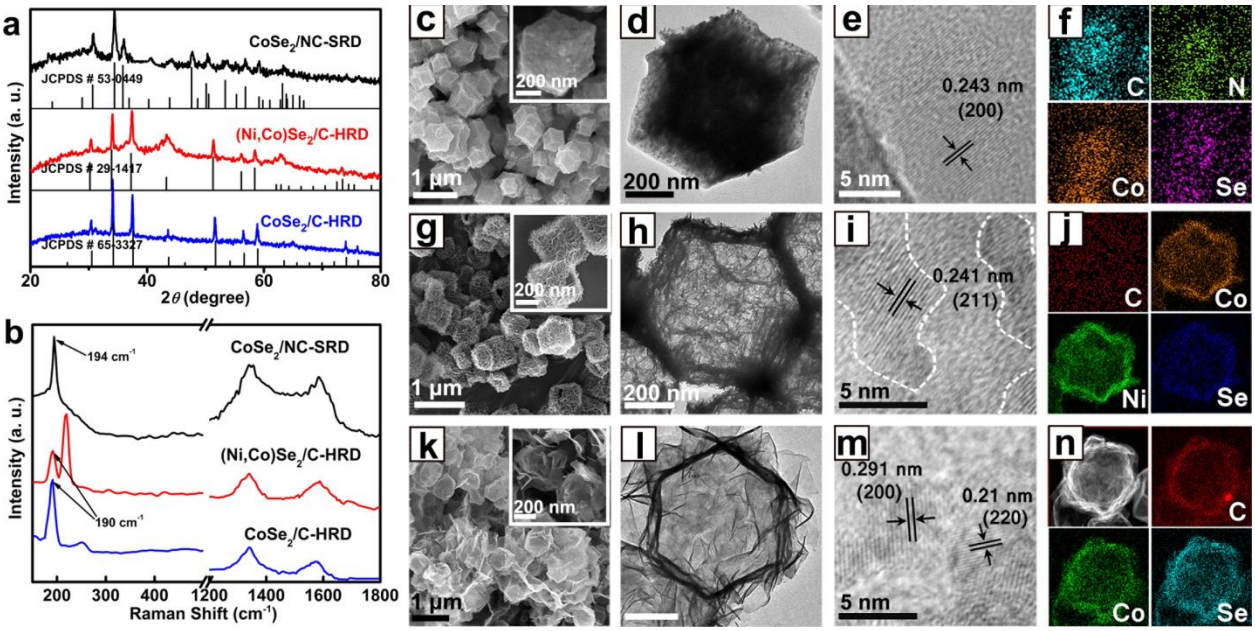

Fig. 2. (a) XRD patterns and (b) Raman spectra of $CoSe_2$/NC-SRD, (Ni,Co)Se_2/C-HRD, and $CoSe_2$/C-HRD. (c, g, k) SEM, (d, h, l) TEM, (e, i, m) HRTEM, and (f, j, n) STEM-EDS elemental maps of the $CoSe_2$/NC-SRD (c-f), (Ni,Co)Se_2/C-HRD (g-j) and $CoSe_2$/C-HRD (k-n).

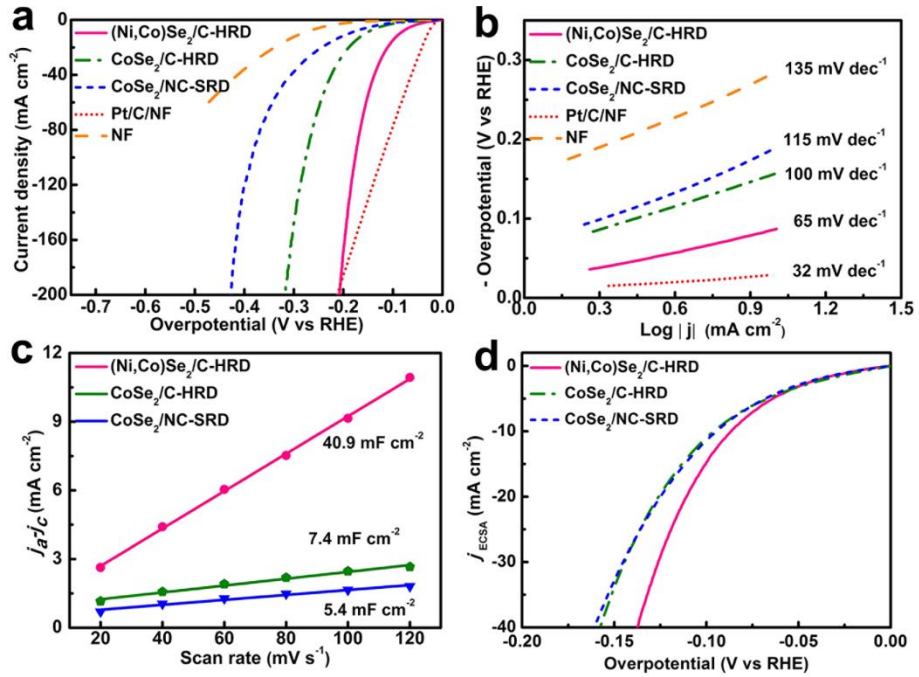

Fig. 3. HER electrocatalysis in 1 M KOH. (a) *IR*-corrected polarization curves of $CoSe_2$/NC-SRD, (Ni,Co)Se_2/C-HRD, and $CoSe_2$/C-HRD for HER. (b) The corresponding Tafel slopes. (c) The difference in anodic and cathodic current density plotted against the scan rate for the determination of the double layer capacitance. (d) Polarization curves normalized by ECSA.

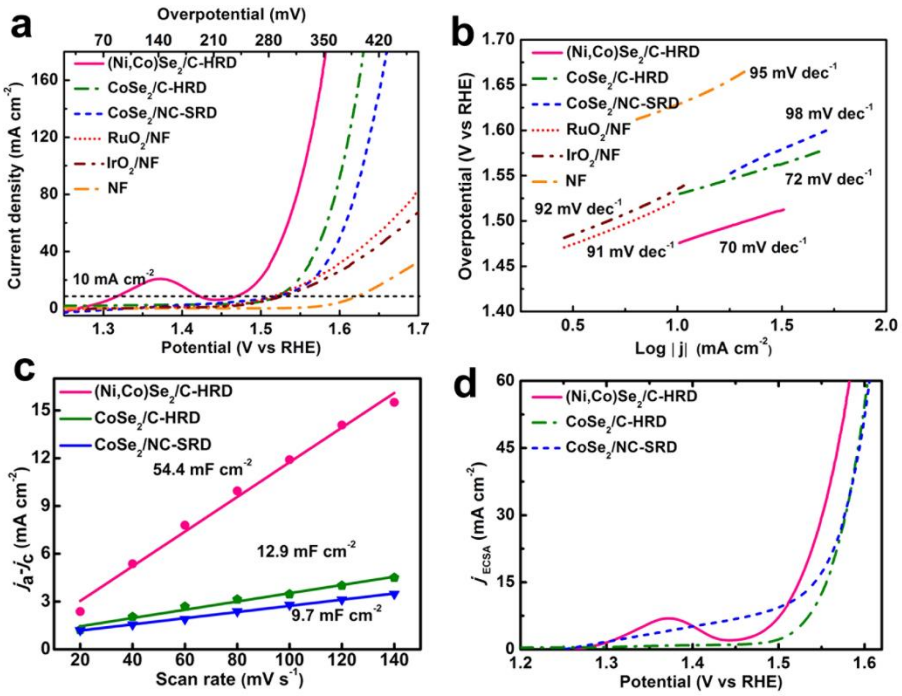

Fig. 4. OER electrocatalysis in 1 M KOH. (a) *IR*-corrected polarization curves of $CoSe_2$/NC-SRD, (Ni,Co)Se_2/C-HRD, and $CoSe_2$/C-HRD for OER. (b) The corresponding Tafel slopes. (c) The difference in anodic and cathodic current density plotted against the scan rate for the determination of the double layer capacitance. (d) Polarization curves normalized by ECSA.

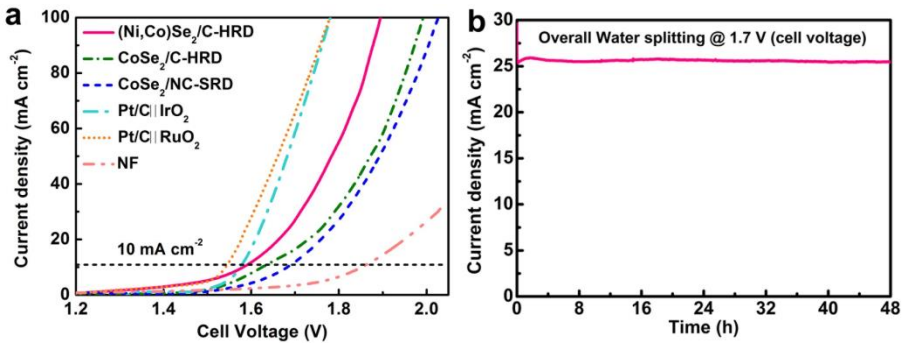

Fig. 5. (a) Polarization curves of RuO_2||Pt/C, IrO_2||Pt/C, $CoSe_2$/NC-SRD, (Ni,Co)Se_2/C-HRD, $CoSe_2$/C-HRD, and NF recorded at a scan rate of 0.5 mV s^{-1} in a two electrode system in 1 M KOH. (b) Time-dependent current density curve for the (Ni,Co)Se_2/C-HRD under a static potential of 1.7 V vs. RHE for 48 h.